EXPERIMENTAL STUDY ON HEAT TRANSFER PERFORMANCE AND FLOW VISUALIZATION IN MICROCHANNELS WITH MICROPILLARS

by

Mingzheng YE[a], Tingxiang YAN[a], Jin WANG[a*], Yongqing HE[b], and Jiri Jaromir KLEMEŠ[c]

[a] School of Energy and Environmental Engineering, Hebei University of Technology, Tianjin, China
[b] Chongqing Key Laboratory of Micro-Nano System and Intelligent Sensing, Chongqing Technology and Business University, Chongqing, China
[c] Sustainable Process Integration Laboratory – SPIL, NETME Centre, Faculty of Mechanical Engineering, Brno University of Technology – VUT Brno, Brno, Czech Republic

Original scientific paper
https://doi.org/10.2298/TSCI2205169Y

This research investigated heat transfer performance and flow characteristics of three polydimethylsiloxane microchannels full of deionised water as a working fluid. A single micropillar, horizontal micropillars, and vertical micropillars along the flow direction were prepared on the microchannels experimentally. Results show that the Nusselt number of microchannels with two horizontal micropillars is 19% higher than that with a single micropillar. The microchannel with two vertical micropillars has the Nusselt number is 29% higher than that with a single micropillar, which shows the best performance on the heat transfer enhancement. Visualization experiments of the flow field were carried out to explore the enhanced mechanism of the heat transfer for microchannels with various micropillar arrangements. When the flow rate is 7 mLpm, the maximum velocities near the single cylinder and the horizontal micro-column are 0.5 m/s and 0.52 m/s. Fluid velocity in a region between two vertical micropillars reaches 0.72 m/s when the flow rate is 7 mLpm. The fluid in the high-speed region is fully mixed around the micropillar, which reduces the stagnation region area downstream of the vertical micropillar and enhances heat transfer.

Key words: *heat transfer enhancement, microchannel, micropillar, particle image velocimetry, stagnation region*

Introduction

For the safe operation of electronic devices, heat dissipation technologies using various microchannels have become an important branch of thermal science. The geometry structure of microchannel heat sinks (MCHS) is a vital factor affecting their heat exchange capability. Dadvand *et al.* [1] investigated the effects of rigid and flexible beams on the thermal performance of a microchannel with a cylindrical obstacle. Results indicated that the flexible beam showed an 18.46% increase in the total Nusselt number compared to the rigid beam. Li *et al.* [2] arranged rectangular ribs on the sides of a smooth rectangular microchannel to im-

* Corresponding author, e-mail: jin.wang@hebut.edu.cn

prove its heat transfer performance. The microchannel with one-side rectangular ribs obtained the highest thermal performance under a volume flow rate of 75 mLpm. Ringkai *et al.* [3] pointed out that a slight increase in the radius of microchannels offered a significant increase in the flow rate of a fluid. Vinoth and Senthil [4] investigated the effects of different inlet cross-sections on the heat transfer performance of MCHS. Results showed that the trapezoidal entrance section has better comprehensive performance than the square and the semicircle sections.

Some studies have mainly focused on enhancing disturbance inside microchannels, and it was recommended to change the geometry structure of microchannels or add ribs to the microchannel wall. Li *et al.* [5] put forward novel MCHS with cavities and fins to increase pressure drop and friction loss due to a disturbance to the boundary-layer. With enhancements of convective heat transfer, the comprehensive performance of complex MCHS is improved compared to that of traditional structures. Erp *et al.* [6] produced an integrated manifold microchannel offered above 1.7 kW/cm^2 heat flux by using a pumping power of 0.57 W/cm^2. It is observed that high rib height showed a large heat transfer in reference [7]. Rezaei *et al.* [8] pointed out that the addition of ribs in microchannels significantly increased both heat transfer and pressure drop.

Nanoparticles have emerged as a strong candidate to increase the thermal conductivity of base fluids. It was testified that the addition of copper nanoparticles enhanced convective boiling heat transfer in a microchannel at a low flow rate [9]. Wang and Li [10] analyzed the effect of nanoparticles on droplet formation in a T-shaped microfluidic device, such as interfacial tension caused by nanoparticles. Zheng *et al.* [11] found that for 1.0 wt.% Fe_3O_4-water nanofluid, heat transfer coefficient in a plate heat exchanger increased by 30.8% at 8 Lpm compared to deionised-water. Anwar *et al.* [12] numerically investigated the effects of fin spacings on the thermal performance of 1.5% CuO-water nanofluids in mini-channel heat sinks and results indicated that 9.1% temperature reduction of base fluid was observed using 0.2 mm fin spacing compared to deionised-water. Siddiqui *et al.* [13] studied cooling rates of water-based Al_2O_3 and Cu nanofluids with 0.251% and 0.11% volume concentrations. With an increase in Reynolds number, Cu-water nanofluid showed better performance than Al_2O_3-water nanofluid. 12.56% increase in overall heat transfer coefficient was obtained for Cu nanofluid. Wang *et al.* [14] investigated the effects of nanoparticle volume fraction on the overall performance factor and overall thermal resistance of an integrated MCHS. Zheng *et al.* [15] investigated thermal performance and pressure drop in a plate heat exchanger filled with ferrofluids under various magnetic fields. Results indicated that 0.1% of ferrofluids showed a 10.0% reduction of pressure drop when two vertical magnets were arranged side by side. Zhou *et al.* [16] experimentally studied the heat transfer effect of microchannels with various micropillars, and results showed that the droplet cylinder has the best heat transfer enhancement with a Nusselt number ratio of 1.6. Lee *et al.* [17] experimentally studied boiling heat transfer in a copper channel with a porous coating. When the heat flux is 51 kW/m^2, the microchannel with the porous coating is 43% higher heat transfer performance than the basic channel.

In order to investigate enhanced mechanisms of heat transfer in electronic devices, flow characteristics of microfluidics in microchannels are necessary to be investigated using micro-particle image velocimetry (micro-PIV) measurements [18]. It can accurately obtain the velocity field of microfluidics and clearly display them through images, so the micro-PIV technique has become a crucial means of microfluid research in microchannels and promoted the research of microfluidics. Li *et al.* [19] explored the flow characteristics of deionised-water

at the inlet section of microchannels using micro-PIV measurements. Xiong *et al.* [20] combined micro-PIV measurements with numerical simulations to analyze the effects of physical properties on fluid flow in microchannels. In this paper, three microchannels are fabricated with different arrangements of micropillars, and heat transfer performance is investigated at different flow rates. In order to explore the mechanism of heat transfer enhancement, a micro-PIV system is set up to carry out visualization experiments of the flow field.

The machining of microchannels is a complex process, and testing data is time-consuming and highly costed. The existing findings on the heat transfer performance of microchannels were mainly conducted numerically. Few studies investigated the heat transfer characteristics of microchannels both from thermal analysis and flow visualization. In this paper, three microchannels are fabricated with different arrangements of micropillars, and heat transfer performance is investigated at different flow rates. In order to explore the mechanism of heat transfer enhancement, a micro-PIV system is set up to carry out visualization experiments of the flow field.

Experimental procedure

This part introduces testing systems for thermal performance and flow distribution.

Experimental system for thermal performance analysis

Figure 1 shows the preparation process of the microchannel. The microchannel is made of polydimethylsiloxane (PDMS). The base liquid and curing agent (Sylgard 184, Dow Corning Corporation, America) are mixed with a ratio of 10:1, and the mixture is put into an empty chamber to discharge bubbles. The mixture is poured into a silicon mould with a hydrophobic surface, which is placed into an incubator (DZF-6050A, Lichen Corporation, China) at 80 °C for 30 minutes. After cooling, the PDMS is carefully removed from the silicon mould. This process allows for the transfer of fine structures from the silicon mould to the PDMS substrate. The PDMS substrate and cover plate are put into an oxygen ionizer (VP-R, Sun June, China) for 1 minute, which is quickly pulled out. The two structures are bonded together. Finally, the inlet and outlet of microchannels are machined by a hole punch.

With a check on the tightness of the test section and data stability, the injection pump (WO109-1B, Longer Pump Corporation, China) is turned on to drain bubbles in the fluid. The DC power supply (MP-3020D, Maisheng Electronics Ltd., China) is turned on for heating the plate. The entire test section is wrapped with thermal insulation cotton to reduce environmental impact. Temperature data is recorded when outlet temperature is stable. Every test is repeated five times.

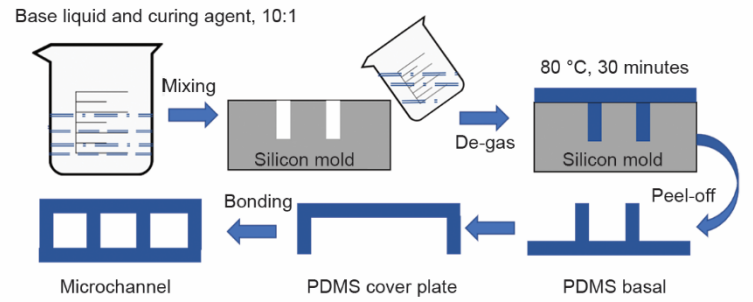

Figure 1. Preparation of PDMS microchannels

Figure 2 shows an experimental system for thermal analysis of a microchannel. The system mainly includes a microchannel test section, injection pump with high precision, heating sheet, DC power supply, data collector and computer. The injection pump allows precise flow control. The T-type thermocouples (TT-30, Omega Engineering Inc., America) are arranged at the inlet, outlet, and bottom of a microchannel. The temperature signal is converted into an electrical signal through a data collector (cDAQ-9181, National Instruments Corporation, America). The electric heating sheet is attached to the bottom of the microchannel. The heating sheet is connected to the DC power to heat the fluid. Figure 2 also shows the test section and three microchannels, *i. e.*, single micropillar two micropillars with horizontal or vertical arrangements (along the flow direction). The microchannel has a width, *W*, of 3 mm, length, *L*, of 30 mm and height, *H*, of 0.1 mm. The micropillar diameter, *R*, is 0.4 mm, and spacing, *d*, between two micropillars is 1 mm.

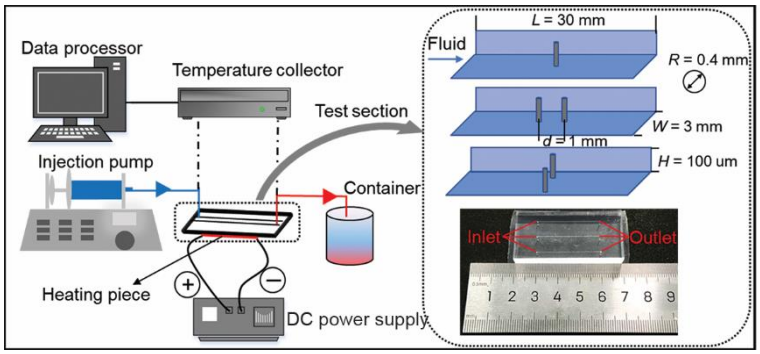

Figure 2. The schematic on thermal performance measurement system of microchannels

Experimental system for flow field testing

Figure 3 shows a micro-PIV testing system, mainly including a flow control system, image acquisition system and image processing system. The flow system consists of a PDMS test sheet, testing fluid, tracer particle and injection pump. Image acquisition system mainly includes double-pulse laser, synchronizer, high-speed charge coupled device camera and high-precision microscope. The image processing system is an image processing computer with the installed software. The transient velocity distribution of the flow field is indirectly calculated by measuring the displacement of the tracer particles in a known time interval. The flow region with tracer particles is illuminated by a laser, and then positions of particles in secondary exposure are recorded by photography or video record. The displacement of each particle is obtained by image analysis technology. Flow velocity at each position is calculated based on particle displacement and exposure time interval. The tracer particles with 2 microns diameter are produced by Duke Scientific Corporation Company, USA. The tracer particles are mixed with deionised water in a ratio of 1:50. Tracer particles emit light with a wavelength of 532 nm under laser illumination. Synchronizer provides a guarantee for accurate image capture as a switch of laser generator and high-speed camera. The test section is placed on a microscope platform. By adjusting the focus of the microscope, the particles are clearly observed in the microchannel. Original and actual dimensions in images are calibrated in software. Micro-PIV measurement principle was introduced in detail [21].

For an analysis of experimental uncertainty, the measurement accuracy of the T-tape thermocouples is ±0.1 K. The flow error of the injection pump is below 1%. The error of the DC power supply is 2%. Based on a calculation, the error of the Nusselt number is below 5%. The error of the micro-PIV measurement system is below 6%.

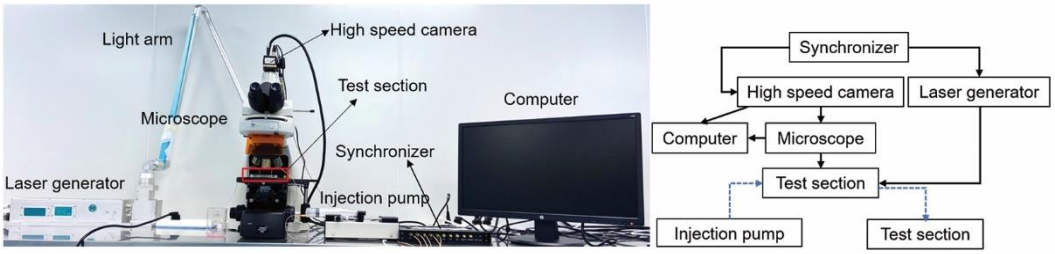

Figure 3. Micro-PIV test system

Results and discussion

A temperature difference of fluid between an inlet and at an outlet is discussed under different flow rates. Visualization flow fields are presented to explain the contribution of flow behavior to heat transfer enhancement.

Heat transfer performance of microchannels

Figure 4 shows temperature differences, ΔT, between the inlet and at the outlet, and fluid temperature at the inlet is set to 293 K. These temperature differences decrease with the increase in the flow rate of the fluid. When the flow rate is above 6 mLpm, the temperature difference decreases slowly at a high flow rate due to a short time to absorb heat. It is found that the microchannel with vertical micropillars has the largest temperature differences at various flow rates. The microchannel with a single micropillar shows the smallest temperature difference of the microchannel. This result indicates that the flow of fluid in the microchannel with vertical micropillars carries more heat fluxes than that in the microchannels with horizontal micropillars and single micropillar. Under the flow rate above 5 mLpm, the temperature difference of fluid in the microchannel with vertical micropillars at 6 W heating power is larger than that with a single micropillar at a heating power of 8 W. When the flow is more than 6 mLpm, the temperature difference of fluid in the microchannel with horizontal micropillars at a heating power of 6 W is larger than that with single micropillar at a heating power of 8 W. These results indicates that the increase in the micropillar (from 1 to 2 micropillars) shows more enhanced heat transfer under low heating power (6 W) than the single micropillar at high heating power (8 W). The temperature difference of the mi-

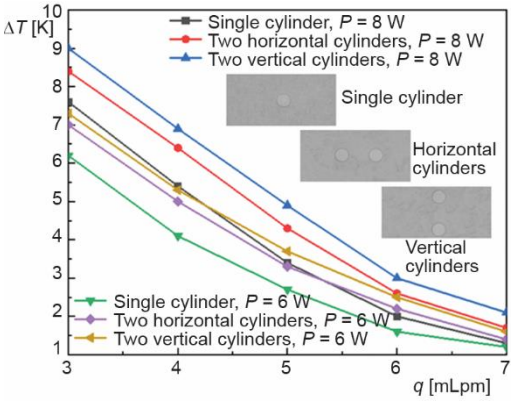

Figure 4. Temperature differences of fluid between inlet and outlet under various flow rates

crochannel decreases with the increase in the flow rate. When the heating power is 6 W, the temperature differences of a microchannel with vertical micropillars at a flowrate of 7 mLpm are close to that with horizontal micropillars. It is concluded that little temperature difference at a high flow rate is observed by changing micropillar number and arrangement on the microchannel at low heating power.

Figure 5 presents variations of Nusselt number for different microchannels, and the Nusselt number and convective heat transfer coefficient are calculated as given in [22]:

$$\mathrm{Nu} = \frac{hD_\mathrm{h}}{k} \tag{1}$$

$$h = \frac{Q}{A\Delta T_m} \tag{2}$$

$$\Delta T_m = \frac{1}{3}(T_1 + T_2 + T_3) - \frac{1}{2}(T_\mathrm{inlet} + T_\mathrm{outlet}) \tag{3}$$

where D_h is the hydraulic diameter of the microchannel, k – the thermal conductivity of the fluid, Q – the heat flux at the microchannel bottom, and A – an area of the microchannel bottom.

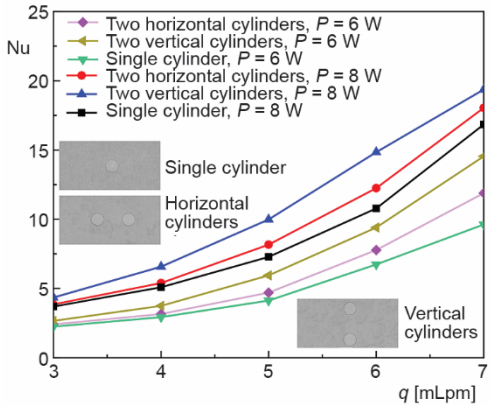

Figure 5. Nusselt number variations in the microchannels with vertical micropillars

The microchannel with vertical micropillars shows the largest Nusselt number at various flow rates. The Nusselt number of the microchannel with horizontal micropillars is larger than that of microchannels with a single micropillar. When the flow rate is 3 mLpm and heating power is 8 W, the Nusselt number for the microchannel with vertical micropillars is 13% higher than that for a single micropillar. The horizontal micropillars have a 4% higher Nusselt number than the single micropillar. When the flow rate is 7 mLpm and heating power is 8 W, the Nusselt number for the vertical micropillars is 15% higher than that for the single micropillar, and the Nusselt number for the horizontal micropillars is 7.4% higher than that for the single micropillar. Under the flow rate of 3 mLpm and heating power of 6 W, the Nusselt number for the vertical micropillars is 18% higher than that for the single micropillar, whereas the Nusselt number of horizontal micropillars is 7.1% higher than that for the single micropillar. Under the flow rate of 7 mLpm and heating power of 6 W, the Nusselt number for the vertical micropillars is 29% higher than that for a single micropillar, whereas the Nusselt number for the horizontal micropillars is 19% higher than that for the single micropillar. Due to enhanced fluid disturbance, the Nusselt number increases by increasing the number of micropillars.

It is concluded that the microchannel with vertical micropillars has better heat transfer performance than that with horizontal micropillars.

Flow characteristics of the fluid in microchannels

Figure 6 shows a physical picture of a microchannel with a single micropillar and velocity contour under flow rates of 3 mLpm, 5 mLpm, and 7 mLpm. Table 1 shows inlet velocities of fluid at different flow rates. Fluid passes over a micropillar, which forms a high-speed zone around the lateral sides of the micropillar. The micropillar intensifies the flow turbulence of fluid. A stagnant zone is formed downstream of the micropillar. The stagnant zone extends with the increase in the flow rate. The fluid is divided into two parts by the micropillar, and fluid mixing is enhanced in the downstream region. Under flowrates of 3 mLpm, 5 mLpm, and 7 mLpm, the maximum velocities on both lateral sides of the micropillar are 0.35 m/s, 0.45 m/s, and 0.5 m/s.

Table 1. Inlet velocity of fluid at different flow rates

Flow rates [mLpm]	Inlet velocity [ms^{-1}]
3	0.17
4	0.22
5	0.28
6	0.33
7	0.39

In the stagnation zone downstream of the micropillar, the fluid velocity is close to zero. The area of the stagnation zone decreases because the convective heat transfer is weakened. Although the single micropillar shows a certain disturbance to the flow distribution, the fluid downstream, the micropillar, is not fully mixed. The area of the stagnation zone downstream of the single micropillar increases significantly with the increase in the flow rate.

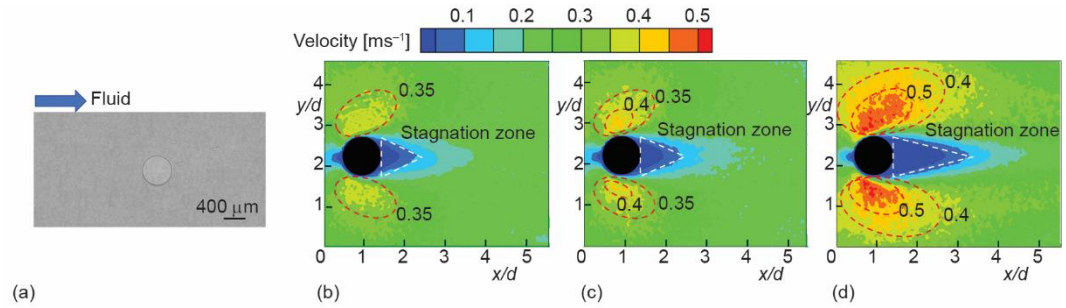

Figure 6. Velocity distributions in the microchannel with single micropillar; (a) microchannel with a single cylinder, (b) q = 3 mLpm, (c) q = 5 mLpm, and (d) q = 7 mLpm

Velocity distributions of a microchannel with horizontal micropillars are presented in fig. 7. The maximum velocities around the micropillar are 0.35 m/s, 0.45 m/s, and 0.5 m/s under flow rates of 3 mLpm, 5 mLpm, and 7 mLpm. Similar results are observed for other those of the microchannel with single micropillar. The back micropillar (the second micropillar) along the flow direction has a slightly lower velocity distribution than the front micropillar. The fluid regions in high velocity are connected and well mixed between two micropillars. The coverage area of high-speed flow in the microchannel with horizontal micropillars is significantly larger than that in the microchannel with a single micropillar. It shows that the convective heat transfer coefficient is improved by the presence of micropillars in the microchannel. Based on the results from figs. 4-6, it is found that the stagnation zone after the back micropillar shows little influence on heat transfer enhancement.

Figure 8 shows velocity distributions in the microchannel with vertical micropillars. High velocities on the lateral sides of the micropillar is 0.5 m/s, 0.6 m/s, and 0.72 m/s at flow

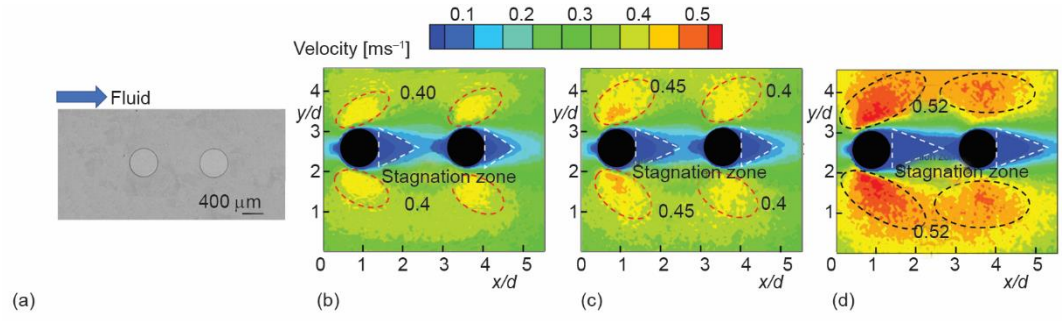

Figure 7. Velocity distributions in the microchannel with horizontal micropillars; (a) microchannel with two horizontal cylinders, (b) q = 3 mLpm, (c) q = 5 mL mLpm, and (d) q = 7 mLpm

rates of 3 mLpm, 5 mLpm, and 7 mLpm. The maximum velocity in the microchannel with vertical micropillars is larger than those with single micropillar and horizontal micropillars. Two vertical micropillars reduce the cross-section area of the microchannel, which results in higher velocity distribution of fluid than other arrangements. Fluid distribution around two vertical micropillars is divided into three parts. One region in high flow velocity is located between two micropillars, which is mainly affected by the interaction between the two micropillars. The convective heat transfer coefficient in the microchannel with vertical micropillars increases significantly because the fluid in the high-speed region is fully mixed. The stagnation zone downstream vertical micropillars are narrowed compared to those single downstream micropillar and horizontal micropillars due to the reduction of the flow cross-section area. It is considered that the vertical arrangement of micropillars shows a significant influence on flow characteristics and heat transfer performance inside microchannels compared to arrangements of single micropillars and horizontal micropillars.

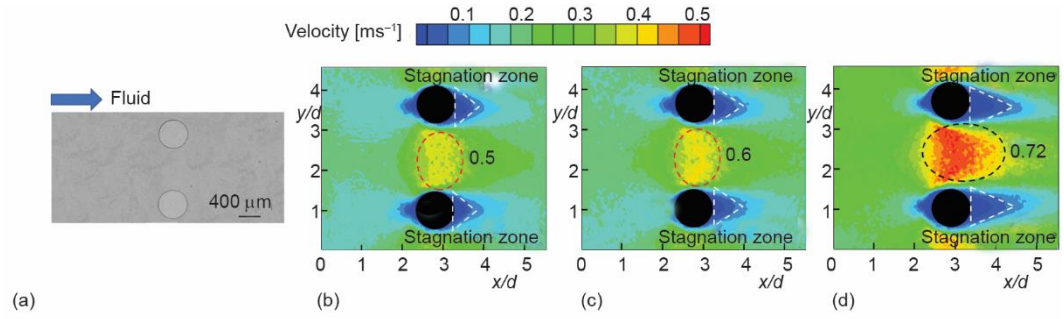

Figure 8. Velocity distributions in the microchannel with vertical micropillars; (a) microchannel with two vertical cylinders, (b) q = 3 mLpm, (c) q = 5 mLpm, and (d) q = 7 mLpm

Conclusions

The effects of micropillars on fluid flow and heat transfer were experimentally investigated in this paper. Thermal performance of microchannels with single micropillars, horizontal micropillars and vertical micropillars was analysed at a flow range of 3-7 mLpm. Results show that the heat transfer performance of microchannels with vertical micropillars is

the highest. Results show that the Nusselt number of the microchannel with vertical micropillars is 29% higher than that with a single micropillar under a flow rate of 7 mLpm and heating power of 6 W. The Nusselt number of the microchannel with horizontal micropillars is 19% higher than that of single micropillar.

Velocity distributions at various flow rates were obtained by using microcosmic PIV. A stagnant zone downstream of the micropillar is extended with the increase in the flow rate. The area of decreases because the weakened convective heat transfer results in the reduction of the stagnation zone. For the vertical arrangement of micropillars, the reduction of the flow cross-section area results in the narrowed stagnation zone downstream vertical micropillars compared to the microchannels with single micropillar and horizontal micropillars.

With the development of micromachining, complex and miniaturized structures were designed and fabricated. We are interested in nanoscale machining methods. The following research will investigate nanoscale effects on flow characteristics and heat transfer enhancement.

Acknowledgment

This work is supported by the National Natural Science Foundation of China (Grant No. 52176067), the Natural Science Foundation of Hebei Province of China (Grant No. E2021202163), the Special Project of Science and Technology Winter Olympics in the Hebei Technology Innovation Guidance Plan (Grant No. 21474501D), and the Project of Innovation Ability Training for Postgraduate Students of Education Department of Hebei Province (Grant No. CXZZSS2021046).

This research was also supported by a project "Sustainable Process Integration Laboratory - SPIL", project No. CZ.02.1.01/0.0/0.0/15_003/0000456 funded by EU as "CZ Operational Programme Research, Development and Education," Priority 1: Strengthening capacity for quality research under the collaboration agreement with Hebei University of Technology, Tianjin, China.

Nomenclature

A – area of microchannel bottom, [m^2]
D_h – hydraulic diameter of microchannel, [m]
h – height of microchannel, [mm]
k – thermal conductivity of fluid, [Wm^{-1}K^{-1}]
Nu – Nusselt number (= hD_h/k), [–]
q – flow rate, [mLpm]
T_1 – the first temperature measurement point on the microchannel bottom, [K]
T_2 – the second temperature measurement point on the microchannel bottom, [K]
T_3 – the third temperature measurement point on the microchannel bottom, [K]
T_{inlet} – inlet temperature of fluid, [K]
T_{outlet} – outlet temperature of fluid, [K]

Acronyms

PIV – particle image velocimetry
PDMS – polydimethylsiloxane

References

[1] Dadvand, A., *et al.*, Enhancement of Heat and Mass Transfer in a Microchannel *via* Passive Oscillation of a Flexible Vortex Generator, *Chemical Energy Science*, *207* (2019), Nov., pp. 556-580
[2] Li, J., *et al.*, Experimental Investigation of the Heat Transfer and Flow Characteristics of Microchannels with Microribs, *International Journal of Heat and Mass Transfer*, *143* (2019), Nov., ID 118482
[3] Ringkai, H., *et al.*, Evolution of Water-in-Oil Droplets in T-Junction Microchannel by Micro-PIV, *Applied Sciences-Basel*, *11* (2021), 11, pp. 1-15
[4] Vinoth, R., Senthil, K. D., Numerical Study of Inlet Cross-section Effect on Oblique Finned Microchannel Heat Sink, *Thermal Science*, *22* (2018), 6B, pp. 2747-2757

[5] Li, Y., *et al.*, Thermal and Hydraulic Characteristics of Microchannel Heat Sinks with Cavities and Fins Based on Field Synergy and Thermodynamic Analysis, *Applied Thermal Engineering*, *175* (2020), July, ID 115348
[6] Erp, R., *et al.*, Co-Designing Electronics with Microfluidics for More Sustainable Cooling, *Nature*, *585* (2020), Sept., pp. 211-216
[7] Akbari, O. A., *et al.*, Investigation of Rib's Height Effect on Heat Transfer and Flow Parameters of Laminar Water-Al_2O_3 Nanofluid in a Rib-microchannel, *Applied Mathematics and Computation*, *290* (2016), Nov., pp. 135-153
[8] Rezaei, O., *et al.*, The Numerical Investigation of Heat Transfer and Pressure Drop of Turbulent Flow in a Triangular Microchannel, *Physica E-Low-Dimensional Systems & Nanostructures*, *93* (2017), Sept., pp. 179-189
[9] Boudouh, M., *et al.*, Experimental Investigation of Convective Boiling in Mini-Channels: Cooling Application of the Proton Exchange Membrane Fuel Cells, *Thermal Science*, *21* (2017), 1A, pp. 223-232
[10] Wang, R. J., Li, Z. H., Influence on Droplet Formation in the Presence of Nanoparticles in a Microfluidic T-junction, *Thermal Science*, *16* (2012), 5, pp. 1429-1432
[11] Zheng, D., *et al.*, Performance Analysis of a Plate Heat Exchanger Using Various Nanofluids, *International Journal of Heat and Mass Transfer*, *158, Part 1* (2020), Mar., ID 119993
[12] Anwar, M., *et al.*, Numerical Study for Heat Transfer Enhancement Using CuO-water Nanofluids Through Mini-Channel Heat Sinks for Microprocessor Cooling, *Thermal Science*, *24* (2020), 5A, pp. 2965-2976
[13] Siddiqui, A. M., *et al.*, Evaluation of Nanofluids Performance for Simulated Microprocessor, *Thermal Science*, *21* (2017), 5, pp. 2227-2236
[14] Wang, J., *et al.*, Effects of Pin Fins and Vortex Generators on Thermal Performance in a Microchannel with Al_2O_3 Nanofluids, *Energy*, *239, Part E* (2022), Jan., ID 122606
[15] Zheng, D., *et al.*, Analyses of Thermal Performance and Pressure Drop in a Plate Heat Exchanger Filled with Ferrofluids under a Magnetic Field, *Fuel*, *293* (2021), June, ID 120432
[16] Zhou, F., *et al.*, Experimental and Numerical Studies on Heat Transfer Enhancement of Microchannel Heat Exchanger Embedded with Different Shape Micropillars, *Applied Thermal Engineering*, *175* (2020), July, ID 115296
[17] Lee, V. Y. S., *et al.*, Flow Boiling Characteristics in Plain and Porous Coated Microchannel Heat Sinks, *International Journal of Heat and Mass Transfer*, *183, Part B* (2022), Feb., ID 122152
[18] Akbaridoust, F., *et al.*, Simultaneous Micro-PIV Measurements and Real-Time Control Trapping in a Cross-slot Channel, *Experiments in Fluids*, *59* (2018), Nov., pp. 1-17
[19] Li, H. W., *et al.*, Experimental and Numerical Investigations on the Flow Characteristics within Hydrodynamic Entrance Regions in Microchannels, *Micromachines*, *10* (2019), 5, pp. 1-20
[20] Xiong, Q. Q., *et al.*, Micro-PIV Measurement and CFD Simulation of Flow Field and Swirling Strength During Droplet Formation Process in a Coaxial Microchannel, *Chemical Engineering Science*, *185* (2018), Aug., pp. 157-167
[21] Wereley, S. T., Meinhart, C. D., Recent Advances in Micro-Particle Image Velocimetry, *Annual Review of Fluid Mechanics*, *42* (2010), Jan., pp. 557-576
[22] Tannehill, J. C., *et al.*, *Computational Fluid Mechanics and Heat Transfer*, Hemisphere Publishing Corporation, Washington, USA, 1984

Paper submitted: February 4, 2022
Paper revised: April 3, 2022
Paper accepted: April 23, 2022